Article

7T Magnetic Compatible Multimodality Electrophysiological Signal Recording System

Jiadong Pan [1],[†], Jie Xia [1],[†], Fan Zhang [2],[†], Luxi Zhang [1], Shaomin Zhang [2], Gang Pan [3] and Shurong Dong [1],*

1   The Key Laboratory of Advanced Micro/Nano Electronic Devices & Smart Systems of Zhejiang, College of Information Science and Electronic Engineering, Zhejiang University, Hangzhou 310027, China; 21960117@zju.edu.cn (J.P.); jiexia@zju.edu.cn (J.X.)
2   The Key Laboratory of Biomedical Engineering of Ministry of Education, Qiushi Academy for Advanced Studies, Zhejiang University, Hangzhou 310027, China; fanz@zju.edu.cn (F.Z.)
3   College of Computer Science and Technology, Zhejiang University, Hangzhou 310027, China
*   Correspondence: dongshurong@zju.edu.cn; Tel.: +86-138-5819-0316
†   These authors contributed equally to this work.

Abstract: This paper developed a comprehensive magnetic resonance imaging (MRI)-compatible electrophysiological (EP) acquisition system, which can acquire various physiological electrical signals, including electrocardiography (ECG), electromyography (EMG), electroencephalography (EEG) and electrocorticogram (ECoG), and EP recording combined with multimodal stimulation. The system is designed to be compatible with the 7-Tesla (7T) ultra-high field MRI environment, providing convenience for neuroscience and physiological research. To achieve MRI compatibility, the device uses magnetically compatible materials and shielding measures on the hardware and algorithm processing on the software side. Different filtering algorithms are adopted for different signals to suppress all kinds of interference in the MRI environment. The system can allow input signals up to ± 0.225 V and channels up to 256. The equipment has been tested and proven to be able to collect a variety of physiological electrical signals effectively. When scanned under the condition of a 7T high-intensity magnetic field, the system does not generate obvious heating and can meet the safety requirements of MRI and EEG acquisition requirements. Moreover, an algorithm is designed and improved to efficiently and automatically remove the gradient artifact (GA) noise generated by MRI, which is a thousand-fold gradient artifact. Overall, this work proposes a complete, portable, MRI-compatible system that can collect a variety of physiological electrical signals and integrate more efficient GA removal algorithms.

Keywords: biomedical equipment; biomedical measurement; signal processing; electroencephalography; functional magnetic resonance

1. Introduction

Magnetic resonance imaging (fMRI) is a noninvasive brain imaging technique that monitors the brain activity of large areas by changes in blood oxygen level-dependent (BOLD) signals [1]. However, BOLD is an indirect readout of brain activity, as it relies on the changes in blood oxygen, which relates to cerebral blood flow, blood volume, and oxygenation [2]. In addition, since the blood oxygenation changes on the order of every few seconds, BOLD cannot detect rapid changes in neuronal activity. Recordings of electrophysiological (EP) signals are a direct way to read the neuronal activity, which has high temporal resolution but limited spatial coverage. Therefore, an advantageous combination of fMRI and EP can overcome their limitations and provide a powerful aid to neuroscience research [3]. With the continuous development of neuroscience and clinical research, a MRI-compatible EP signal acquisition system enabling simultaneous fMRI and EP is necessary to meet the needs of multiple applications. In 2019, a multimodal ultra-high field (7T) fMRI study was conducted to investigate the effects of breathing under auricular vagus stimulation on

the brain stem and cardiovascular responses, which included electrocardiography (ECG) and other biological signals [4]. In 2019, the quantitative determination of concordance in localizing the epileptic focus by component-based electroencephalography (EEG)-fMRI was investigated [5]. An increasing number of studies are using ECG, electromyography (EMG), EEG and electrocorticogram (ECoG) in MRI to provide additional biological information, both for temporal and spatial resolutions [6–8]. So far, some commercial MRI-compatible EP signal acquisition equipment has the following problems: limited type of EP signal, non-portability, no acquisition during MRI scanning, low intensity of compatible MRI, inability to enter the cabin, etc. In addition, commercial MRI-compatible EP signal acquisition devices do not yet have the tools to remove gradient artifacts [9].

Due to the ultra-high static magnetic field, rapidly changing gradient magnetic field and radio frequency field in the MRI environment, the work of bioelectric recording equipment in the magnetic field will face tough challenges. In order to make an EEG acquisition setup compatible with an fMRI environment, the following issues need to be addressed: (1) The material of the equipment should be compatible with the MRI environment, which will not be adsorbed by the strong magnetic field nor affect the uniformity of the static magnetic field. (2) The device shall suppress the voltage signal amplitude entering the analog-to-digital converter (ADC) and ensure that the dynamic range of the voltage that can be collected by the device shall be greater than the amplitude range of the EEG signal with the gradient artifact superimposed and leave a certain margin to ensure that saturation distortion will not occur, so that the subsequent data processing can restore a clean EEG signal [10]. (3) The equipment needs to filter out the radio frequency (RF) interference signal generated by the MRI transmitting coil [11]. (4) The equipment needs to solve the problem of eddy current heating caused by the change in the gradient magnetic field in the metal material in contact with the human body [12]. (5) The device shall be equipped with a gradient artifact (GA) removal algorithm to restore a clean EEG signal [13–15]. Gradient magnetic fields induce currents in electrodes and wires, creating gradient artifacts. The amplitude of the gradient artifact is usually more than 1000 times that of the EEG signal, and its frequency band overlaps with that of the EEG signal. Therefore, the large-scale artifact signal will drown the EEG signal, and it is difficult to remove directly by a simple filter. In the MRI environment, artifact signals can be collected by additional channels and then directly removed by algorithms [16–19]. However, these efforts target specific types of bioelectricity or lack systematic integration, making it unable to adapt to various applications and the growing demand for converged technologies. Niazy et al. proposed the optimal basis algorithm to remove gradient artifacts [20]. The core of the algorithm is to remove most of the gradient artifacts by using Average Artifact Subtraction (AAS) proposed by Allen [16] and then analyze the main components of the signal to further remove the gradient artifacts. The main method of AAS to remove the gradient artifact is to construct the template of the gradient artifact and then subtract the artifact template from the original signal to obtain a clean EEG signal. In recent years, more and more machine learning and deep learning algorithms have been applied to EEG processing, as well as more and more research towards the automatic removal of gradient artifacts [21–24]. Duffy et al. first used denoising autoencoders (DAE) to remove gradient artifacts for simultaneous EEG-fMRI automatically [25]. Since the amplitude of the gradient artifact is hundreds of multiples of EEG and ECG, the effect of removing artifacts is poor, and the root mean squared error (RMSE) is large (40.2). Therefore, we propose a new GA removal method, which converts the input data format based on DAE. The RMSE of the new algorithm is 0.13.

We here designed an EP signal acquisition system that can work simultaneously with MRI under an ultra-high magnetic field. This is a complete system, including acquisition equipment, signal processing software and matching artifact removal algorithms designed for a variety of EP signals. The system has excellent performance, the input noise is lower than 1 μVrms, the dynamic range of the input is ±225 mV and the number of channels can reach 256. More importantly, its portability makes the acquisition experiment environment more extensive and convenient. The acquisition and digitization can be completed in the

MRI chamber to improve the signal quality. Throughout this system, different electrodes can be used to simultaneously collect bioelectrical signals from different parts, like ECG, EMG, EEG and ECoG. Moreover, high-density applications can be designed with their multichannel advantages, which will provide a lot of convenience for the varied application occasions in neuroscience research and clinical research.

2. Materials and Methods

2.1. System Architecture

The structure of the EP signal acquisition system has two parts: hardware and software. The hardware consists of six parts: (1) ESD protection unit; (2) anti-aliasing filter; (3) amplifier and analog-to-digital converter; (4) MRI sync clock; (5) microcontroller; (6) optical fiber transmission module. The software contains three parts: (1) microcontroller code to implement hardware control and data communication; (2) data display and processing software to realize data communication, processing, and display; (3) gradient artifact removal algorithm. The block diagram of the EP signal acquisition system, device appearance and host computer display is shown in Figure 1.
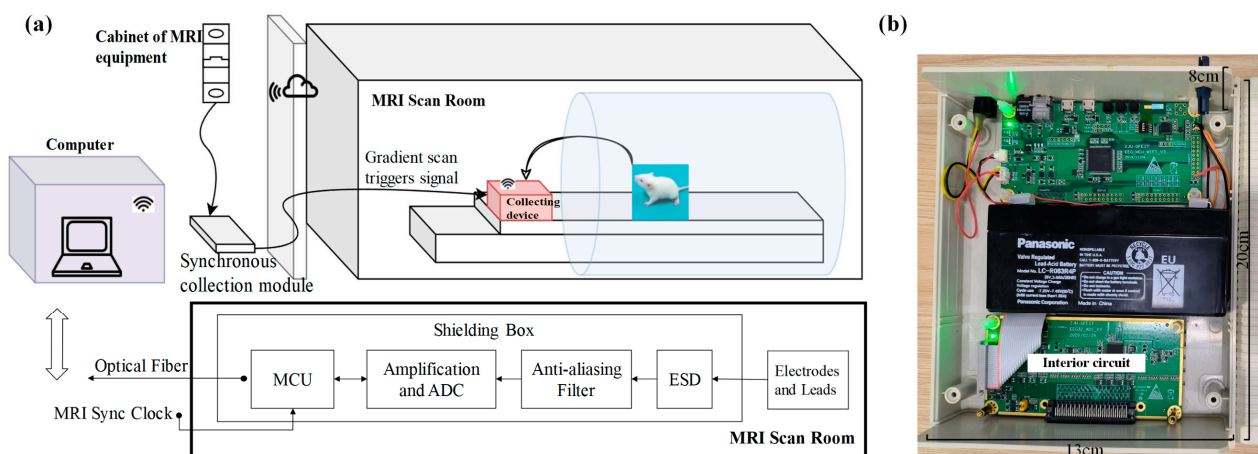
Figure 1. (**a**) Block diagram of system. (**b**) EP signal acquisition system and shielding box (20 cm × 13 cm × 8 cm).

2.2. Hardware of EP Signal Acquisition System

The hardware composition of the acquisition system is divided into three parts: acquisition module, main control module and transmission module. The acquisition module utilizes the ADS1299 bioelectric acquisition chip from TI, which has an 8-channel capacity and features ESD protection and anti-aliasing filter circuits. This module performs signal amplification and analog-to-digital conversion, as well as electrode shedding detection, bias drive circuit output and single-/double-electrode connection switching functions. The main control module is composed of microcontroller ATSAMS70N20A, which controls the acquisition module and transmission module. The latter is composed of the ATWINC1510 wireless transmission module that enables wireless data transmission. The schematic diagram of the overall acquisition system composition is shown in Supplemental Note S1.

Before entering the ADC, ESD protection is performed on the EP signals. The bi-directional transient voltage suppression diode array is employed to safeguard against electrostatic hazards that may be caused by the frequently inserted lead wire connectors. The amplifier and ADC use the ADS1299 chip, which features a 24-bit ADC capable of simultaneously acquiring 8-channel signals at a rate of up to 16kSPS. Equipped with a low-noise amplifier, the highest gain is 24 V/V. Its ADC utilizes oversampling technology with an actual adoption rate half of the chip clock, up to 1.024 MHz. The high oversampling rate allows for only a simple first-order RC low-pass filter to achieve the anti-aliasing effect, with a cut-off frequency of 6.79 kHz (R = 4.99 kΩ and C = 4.7 nF) and stopband attenuation greater than 40 dB. Four ADS1299 chips are daisy-chained to enable the simultaneous

acquisition of 32-channel signals, with support for multiple 32-channel acquisition boards overlay up to 256 channels (The method is shown in Supplemental Note S1).

Regarding collection methods, the single-electrode connection method is utilized in EEG signal collection, with all channels sharing a reference electrode. The two-electrode connection method is used in EMG signal acquisition, with independent N and P differential inputs for all channels. To accommodate these different acquisition methods, the acquisition device is capable of switching between single-/double-electrode connections and controlling whether the same reference electrode is shared. ADS1299 provides functions such as single-/double-electrode switching, real-time wire break detection and bias drive output, which are necessary for electrode contact condition monitoring and common mode noise reduction during EEG and EMG acquisition. These functions are retained and supported in the software and hardware used in this study.

Supplemental Table S1 shows the diverse signal characteristics. The amplitude of the EEG signals ranges from a few microvolts to dozens of microvolts, while the maximum amplitude of the EMG signals can reach a few millivolts but generally does not exceed 1 mV. Therefore, amplifiers and analog-to-digital converters with a dynamic range greater than ± 10 mV can meet the amplitude requirements. The main energy distribution of the EEG signals is between 0 and 50 Hz, and the main energy distribution of EMG is between 20 and 150 Hz. Therefore, ADC with a sampling rate above 300 Hz can meet the frequency requirements. The dynamic range of the acquisition chip differential mode input voltage is ± 4.5 V at no gain and ± 225 mV at 20 times gain, and the sampling rate can reach up to 16k SPS, which satisfies the requirements.

The technical indicators are shown in Supplemental Table S2, and the performance parameters are compared with commercial types of equipment in Table 1. The acquisition device designed in this study achieves 256-channel high-density acquisition and wireless transmission and innovatively integrates EEG and EMG acquisition. Other performance indicators are similar to or even better than those of commercial devices. In addition, the system also has magnetic compatibility and small portable performance. A magnetically compatible active preamplifier for various magnetically compatible electrodes and a MRI synchronous acquisition module for EPI signal synchronization were also made to facilitate EEG signal acquisition under 7T MRI (Supplemental Figure S1).

Table 1. Technical specifications.

Parameter	Brain Product BrainAmp MR	NeuroScan SynAmps	Delsys Trigno Tiber	TDT PZ5	Our Work
EP signal compatible	EEG	EEG	EMG	EEG/EMG	EEG/sEMG/ECG
Number of channels	32	Up to 256	64–128	64–128	Up to 256
Sample rate	5 k	Up to 20 k	2 k	750–50 k	UP to 16 k
ADC bit	16	24	16	16	24
CMRR	−90 dB	−110 dB	−80 dB	−104 dB	−110 dB
Input noise	<1 μVpp	<0.5 μVpp	<1.5 μVrms	3.0 μVrms 300–7 kHz	<1 μVrms
Bandwidth	0–250 Hz	0–3.5 kHz	10–450 Hz	0.1–10 kHz	0–6.8 kHz
Input impedance	10 MΩ	10 GΩ	/	/	>500 MΩ
Acquisition methods	Single-electrode	Single-/dual-electrodes	Single-electrode	Single-/dual-electrodes	Single-/dual-electrodes
Filter	Butterworth	/	/	low-pass, notch, bandpass	8-order low-pass, notch, bandpass
Dynamic voltage circumference	±16.384 mV	±400 mV	±11 mV	±0.5 V	±0.225 V
Data transmission	optical fiber	Passive carbon fiber	USB/Wi-Fi	wired	Wi-Fi and optical fiber
Access to the MRI	Only amplifier	/	/	Only amplifier	All part
MRI intensity adaptation	3T	4T	/	7T	7T
Collection during MRI scan	√	√	/	√	√
GA removal algorithm	/	√	/	/	√

2.3. Magnetic Compatibility Processing

2.3.1. MRI-Compatible Component Material Selection

In the magnetic field, the magnetic inductance line will be refracted at the interface of different media, resulting in the deviation of the magnetic inductance line. Therefore, in the fMRI environment, metals with similar permeability to air should be used to avoid obvious damage to the static magnetic field uniformity. Given the difficulty in obtaining and processing materials, copper and aluminum are the metals of choice for use in fMRI environments. The pins of common devices are usually doped with ferromagnetic nickel components to improve their mental strength and increase the number of repeatable welds. In the magnetic field, the metal nickel can be adsorbed by the magnetic field, and at the same time, it will change the direction of the magnetic inductance line, affecting the static magnetic field uniformity. Therefore, we customized MRI-compatible resistance vessel parts. The internal electrical connection is made of metallic copper, and the pin is plated with silver copper, without nickel, iron and other ferromagnetic metals. All devices are powered by a 6 V lead–acid battery which contains acid, lead and their compounds. The terminals are made of copper. Lead and copper have similar magnetic permeability to air and will not affect the homogeneity of the static magnetic field, nor be absorbed by the static magnetic field. All other parts of the system are made with magnetically compatible materials such as copper, gold and magnetically compatible polymers.

2.3.2. Magnetic Shielding: EEG-fMRI Synchronous

EEG functional magnetic resonance study scenarios involve the acquisition of EEG electrical signals in a strong magnetic environment, so it is very important for the safety and stability of the acquisition system. This experiment was conducted in a 7T ultra-high field magnetic resonance environment, with a high-intensity static magnetic field, gradient magnetic field during the scanning period of the magnetic resonance sequence and RF field under the RF line country pulse. To shield the RF interference in MRI scanning and to restrain the heating effect of the rapidly changing gradient magnetic field on the hardware, this study uses aluminum to make a shielding box. The aluminum box functions as a Faraday cage to protect the device from external electric fields. Additionally, the gradient magnetic field can induce magnetic fields in opposite directions on the complete metal aluminum plate, which cancel each other out and reduce the strength of the gradient magnetic field inside the device. As for the static magnetic field in MRI, it is not necessary to shield the static magnetic field, because the static magnetic field does not generate energy in a non-ferromagnetic conductor like a gradient magnetic field, as long as the device does not contain ferromagnetic materials that can be attracted by the static magnetic field and damage the MRI device. Moreover, RF refers to the signal that can be radiated into space as an electromagnetic wave, its frequency range is 20 KHz~300 GHz and the cut-off frequency of the anti-aliasing low-pass filter at the front end of the acquisition system is 6.77 kHz, so the thousands of disturbances to the EEG signal can be eliminated. The GA caused by the gradient magnetic field is removed by the artifact removal algorithm. In addition, under the influence of a strong magnetic field, the electrode leads have a great common mode interference signal. We use a masking driven approach to eliminate interference. After the common-mode signal is obtained in the preamplifier, the shielding layer of the electrode lead is directly driven through the voltage follower instead of grounding, thus eliminating the influence of distributed capacitance.

2.3.3. High-Speed Serial Port—Fiber Optic Design

Due to the limitation of live equipment in the MRI environment, the router cannot be placed in the scanning room. The synchronous optical trigger clock of the MRI scan sequence is converted to an electrical pulse and collected by the MCU, then packaged and sent with the collected EP signal data. This signal is used by the GA removal algorithm to synchronize artifact averaging.

The final system is portable and can fit inside a cabin with a volume reduced to 20 cm × 13 cm × 8 cm, which can enter the MRI room. It has irreplaceable advantages with the popular magnetic-compatible EEG equipment on the market and provides more possibilities for EEG acquisition under fMRI.

2.4. Software of the EP Signal Acquisition System

2.4.1. Data Preprocessing

In the hardware part, we obtained the voltage data collected by ADS1299 and sent the packet serial number, marking data, voltage data and shedding data group packets to the computer through Wi-Fi. The computer-side GUI program is responsible for Wi-Fi data receiving and parsing, data processing, data display and data storage. We used C++ to write GUI programs under the QT platform. Qt Creator is a cross-platform integrated development environment that supports Linux, Windows and MAX OS. Qt is a C++ graphical user interface application development framework. GUI displays the time domain diagram of the collected bioelectrical signal in real time, with an adjustable amplitude and time base. At the same time, GUI calculates the maximum, minimum and root mean square values in real time to display at the upper-right corner of the waveform. GUI provides the function of modifying the number of channels and sampling rate, freely selecting the channels to be displayed, switching between a single-electrode connection and double-electrode connection and the debugging function of sending a single instruction and receiving feedback. In storage, the received data are automatically stored in the program path. The upper limit of file storage is 75 MB. If the upper limit is exceeded, the system automatically creates new files to continue storage. Data processing of the upper computer includes three parts: (1) bandpass, low-pass and 50 Hz notch filters; (2) FFT calculation and real-time display of the FFT analysis results with a refresh frequency of 1 s and frequency resolution of 1 Hz; (3) RMSE value, minimum value and maximum value calculations. Figure 2 shows the GUI interface. The GUI supports the integration of abnormal detection, periodicity, typical pattern, recursion, automatic pre-segmentation and other functions into the more convenient processing of EP signals [26,27].
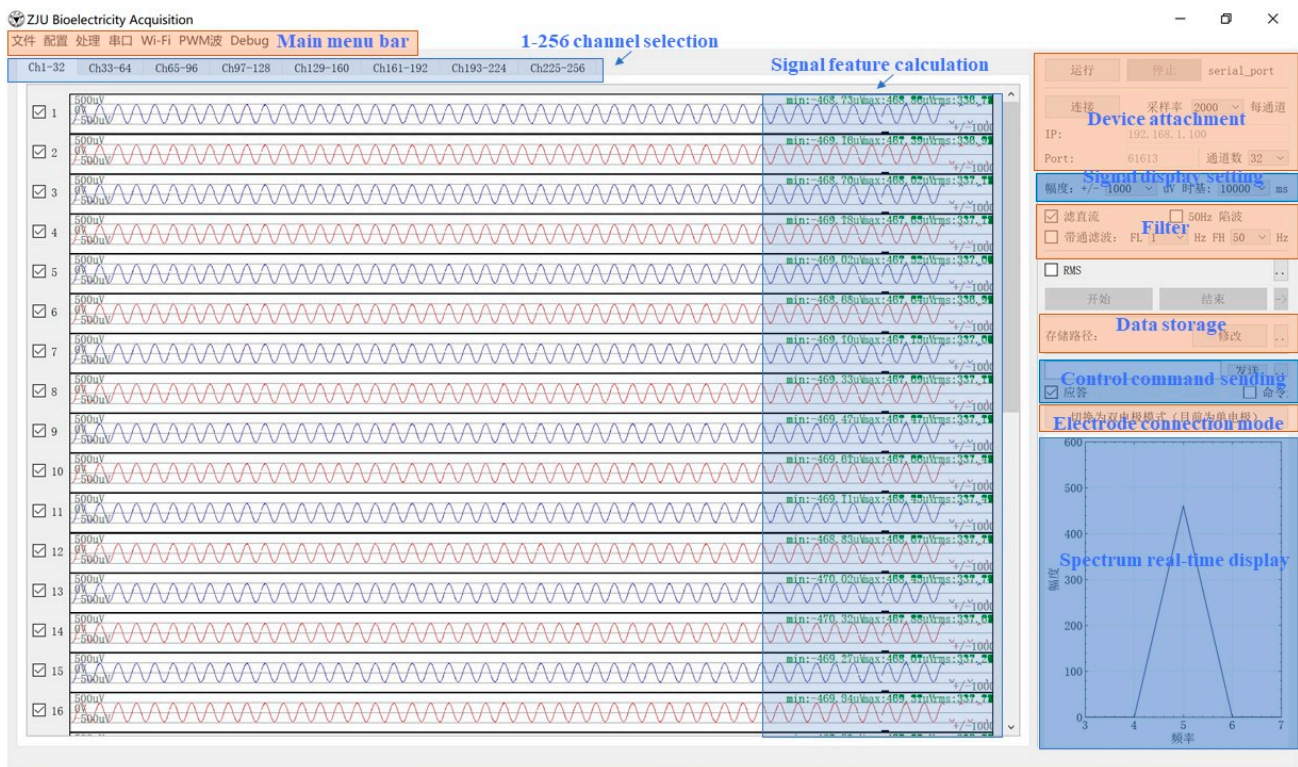

Figure 2. GUI interface.

2.4.2. Artifact Removal

When performing simultaneous fMRI and electrophysiological signal recording, there will be various artifacts, mainly (1) artifacts caused by gradient magnetic fields, (2) artifacts caused by radio frequency fields and (3) artifacts of other electrophysiological signals, such as a cardiac pulse signal. The high-frequency interference introduced by the RF transmitting coil is much higher than the required EEG signal, which can be easily filtered out by the low-pass filter. Since the frequency of the radio frequency field needs to excite the resonance of the atom, which is equal to the Larmor frequency of the atom in a specific static magnetic field, the formula is as follows:

$$f = \frac{\gamma}{2\pi} B_0 \tag{1}$$

where f is the Larmor frequency of the atom, $\gamma/2\pi$ is the atomic gyro ratio and B_0 is the static magnetic field strength. It can be calculated that the RF frequency at the 7T static magnetic field strength is 298.2 MHz. This frequency is much higher than the EP signal frequency, and the RF field artifacts can be reduced effectively by a software low-pass filter. Because of the fixed waveform of ECG artifacts, the ECG reference signal can be collected through additional channels and then removed by the regression method or by blind source separation methods such as an adaptive filter [28] and independent component analysis (ICA) [29]. The pollution source studied in this paper is the gradient artifact, and its processing code is combined with the host computer, which becomes a part of the acquisition system.

AAS is the most widely used gradient artifact removal method. The main method of removing gradient artifacts by AAS is to construct a gradient artifact template and then subtract the artifact template from the original signal to obtain a clean EEG signal. It depends on two preconditions. The first is that the gradient artifacts in adjacent data slices are the same. The second is that EEG signals can cancel each other when averaging, so that the constructed artifact template does not contain EEG signals. The gradient artifact is caused by the variation of the gradient magnetic field of the nuclear magnetic resonance (NMR) instrument, and the gradient magnetic field changes regularly. During a whole brain scan, the gradient magnetic field changes at a fixed interval. Therefore, adjacent gradient artifacts have a high degree of similarity. Usually due to head movement, heartbeat pulse and other reasons, the similarity of adjacent gradient artifacts will decrease.

The DAE can process nonlinear data, accept different types of physiological signals and burst signals and is not limited to the traditional AAS method, which requires strict synchronization and fMRI scanning information. The DAE has the advantages of automation, fast speed and being customizable and interpretable. Since the amplitude of the gradient artifact is hundreds of multiples of EEG, the RMSE is 40.2 [21]. Under different types of scanning, even the position direction of the collecting electrode will produce gradient artifacts with great amplitude differences. Therefore, a more extensive automatic model needs to be proposed.

Therefore, we propose the LOGDAE method, which converts the input data format based on DAE. The raw data mixed with GA noise is first an absolute value and then a logarithmic calculation. During the absolutization, the symbolic data layer (composed of 0 and 1) is added as the plus and minus sign of the recorded data to return the signal of the correct symbol at last. The diagram of the LOGDAE model is shown in Figure 3. We used two layers of DAE to learn double-coding and decoding. The encoder structure and training results are described in detail in Supplemental Figure S2. The experimental results show that LOGDAE has advantages in GA noise removal and achieves an RMSE value of 0.13. This is a brilliant idea of logarithmic processing data to reduce the magnitude difference between the noise and real EEG amplitude, so that weak EEG signals can be learned in the subsequent entry into the DAE.
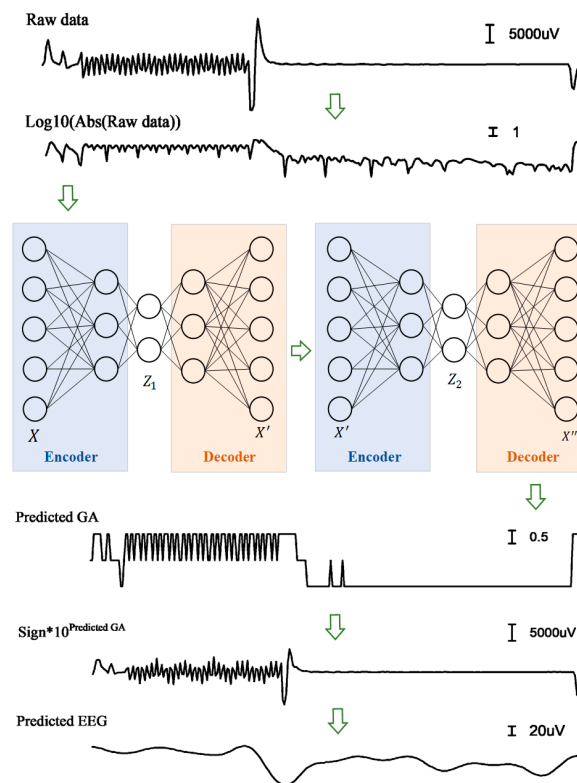
Figure 3. The diagram of the LOGDAE model. "*" in the "Sign*10$^{Predicted\ GA}$" stands for multiplication.

3. Experimental Results

By recording ECG, EMG, EEG and ECoG signals, we verified the device's ability to record multiple EP signals. Furthermore, there are strong magnetic fields, alternating magnetic fields and radio frequency fields in the nuclear magnetic resonance environment, and there is a high demand for equipment performance. In this work, the acquisition device was placed in a MRI device and worked simultaneously with MRI.

3.1. Multitype EP Signals Acquisition

We conducted experiments to verify the effectiveness of ECG, EEG, EMG and ECoG signal acquisition. We confirmed the feasibility of obtaining ECG signals by collecting ECG from monkeys (experimental methods and signals are shown in Supplemental Figure S3). We recorded surface EMG signals during fist clenching using four electrodes placed on the radial and flexor muscles of the right arm, as shown in Supplemental Figure S4. Additionally, we verified the effectiveness of EEG by measuring alpha wave changes during eye-opening/eye-closing experiments in humans. ECoG signals have also been obtained by this recording system from rats and mice brains under multimodal stimulation. The ability to accurately detect multitype EP signals and the portability of the recording system demonstrate its broad application prospects for disease diagnosis and clinical treatment.

3.1.1. Alpha Wave Recording of EEG

The alpha brainwave is one of the four basic brainwaves (alpha, beta, delta and theta) and has a frequency range between 8 and 13 Hz. Alpha waves appear during periods of emotionally stable rest or meditation, particularly when in a calm state. When the eyes are opened, alpha brain waves are suppressed, but when the eyes are closed, they begin to appear. To detect alpha waves, we placed an electrode at O1 (following the International 10–20 system), where the alpha signal is more prominent, along with a reference electrode and a ground electrode at Cz and the earlobe, respectively, as shown in Figure 4a. The subject sat in a comfortable position in a dark, quiet room and relaxed all muscles. Initially,

the subject's eyes were open and closed his eyes after receiving the eye-closing instruction. We set the sampling rate to 1000 SPS, gain to 24 V/V and used an eighth-order 1~70 Hz bandpass filter and 50 Hz notch. The time domain signal obtained is shown in Figure 4, which clearly demonstrates significant differences in the waveforms under open and closed eyes conditions. By applying short-time Fourier changes, a time–frequency domain diagram was generated that revealed the significant appearance of alpha wave bands after the eyes were closed. This finding provides evidence of the EEG acquisition ability of the system.
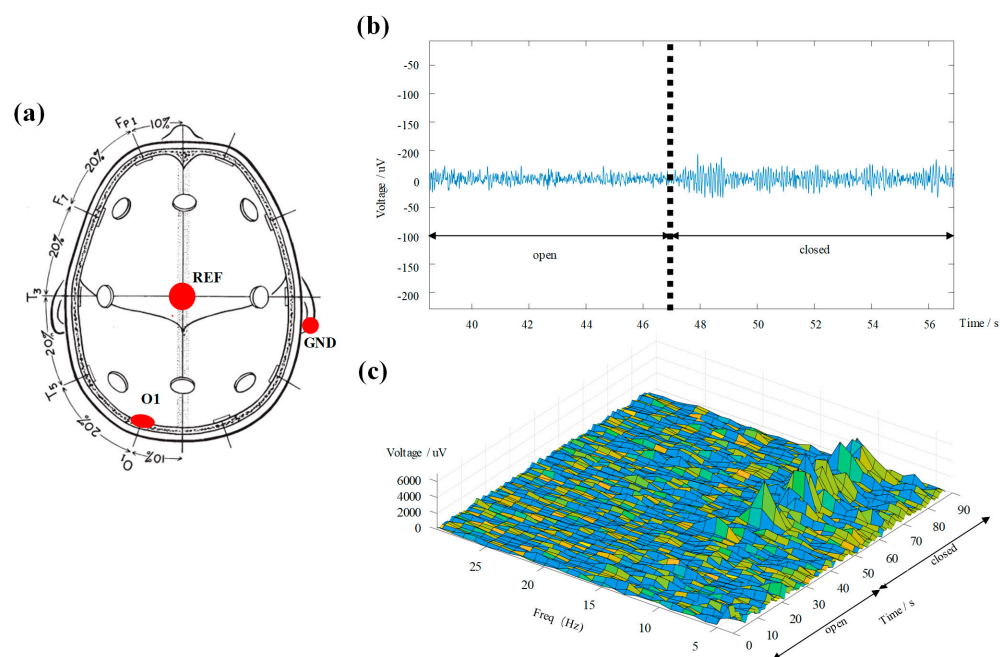

Figure 4. Electrode sites and recorded signals. (**a**) The 10–20 electrode system, O1 for recording, Cz for reference and earlobe for ground. (**b**) Time domain signal before and after closing of the eyes. (**c**) Frequency domain signal before and after closing of the eyes.

3.1.2. ECoG Recording Combined with Multimodal Stimulation

The EP signal acquisition system enables the simultaneous recording of electrophysiological signals from the brain during multimodal stimulation (electrical or light stimulation). Somatosensory evoked potentials (SEPs) are signals recorded from the sensorimotor cortex evoked by peripheral nerve stimulation [30]. We used an electrical stimulator to stimulate the musculus gastrocnemius and tibialis anterior of rats and collected SEPs from a cranial nail implanted on the contralateral primary somatosensory cortex (Figure 5a). The EP signal acquisition system recorded SEPs following unidirectional pulse stimulations (0.1-ms pre-phase, 2-mA current). Figure 5c shows a recording of SEP averaged from 200 trials, which exhibits large and continuous peaks following electrical stimulation, consistent with the characteristics of SEPs [30].

Optogenetics is a technique that can precisely regulate the activity of neurons or other types of cells through light and has been widely used in animal behavior and physiological research. The recording system can be combined with optogenetics to facilitate brain science research. Channelrhodopsin-2 (ChR2) is a blue light-activated cationic channel commonly used in optogenetics [31]. Using 473-nm blue light to activate cortical neurons transfected with the CHR2 virus in the S1 cortex of mice, a typical light-evoked signal was recorded using a transparent electrode [32] and EP signal acquisition system in Figure 5b–d. As photo stimulation was turned on, a large negative peak was recorded, and the signal slowly returned to baseline after the stimulation ended.
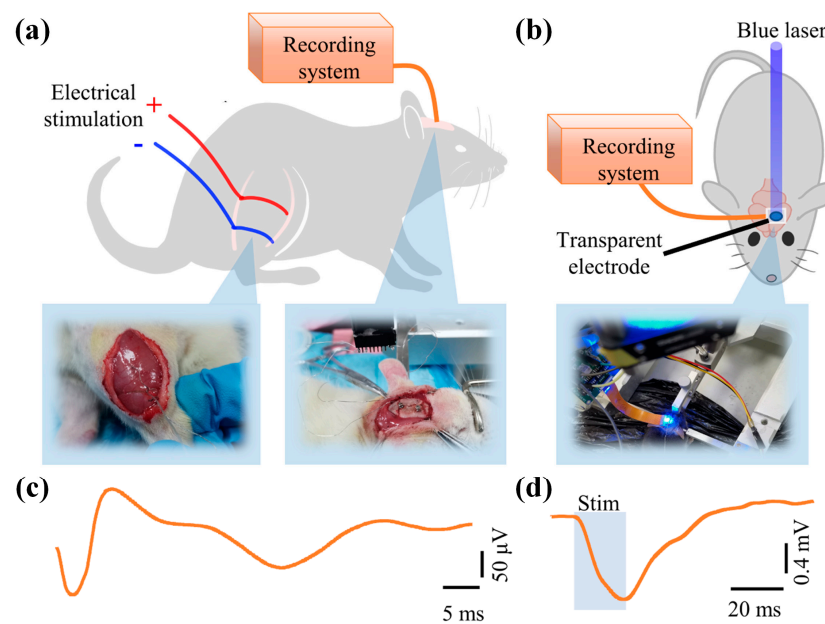
Figure 5. Experimental implementation diagram. (**a**) Stimulated ECoG acquisition from a cranial nail implanted on the contralateral primary somatosensory cortex. (**b**) Using 473-nm blue light to activate cortical neurons transfected with the CHR2 virus in the S1 cortex of mice. (**c**) A recording of SEP averaged from 200 trials by electrical stimulation experiments. (**d**) A recording of averaged SEP by light stimulation experiments.

3.2. Acquisition Experiment in 7T MRI

There are strong magnetic fields, alternating magnetic fields and radio frequency fields in the nuclear magnetic resonance environment, and there is a high demand for equipment performance. In this work, the acquisition device was placed in a MRI device and worked simultaneously with MRI. In a 7T environment, a carbon fiber–graphite electrode was used to record the ECG of the monkey, a PEDOT:PSS electrode to record the sinusoidal signal generated by a physiological signal generator (shown in Supplemental Figure S5) and a comparison with TDT (designed by Tucker-Davis Technologies) for epilepsy signal acquisition in 7T.

### 3.2.1. Heart Rate Monitoring by ECG in 7T MRI

We collected the ECG signals from the monkey during the 7T MRI scan. In this experiment, the standard ECG position V4 in the monkey was shaved and coated with conductive paste, carbon fiber graphite electrodes were attached to the surface and the medical tape was wound and fixed. The time domain signal is shown in Figure 6a. The red line represents the slice timing signal. After 46.6 s, the EPI sequence scan starts, and the collected signal is superimposed with large gradient artifacts; its peak value reaches 1 mVpp. One EPI sequence scan was performed for 38 whole brain scans, each with a total brain scan time of 3000 milliseconds and an interval of 500 milliseconds. Each whole brain scan was divided into 25-layer scans with an interval of 100 ms. Fourier-transform was applied to the signal obtained in the EPI scan sequence, and the frequency domain diagram is shown in Figure 6b,c. The frequency components of the gradient artifact appear in the form of frequency pulses at fixed intervals on the frequency axis, and there is a dominant frequency of the gradient magnetic field switching at 710 Hz. Using the gradient artifact removal algorithm LOGDAE proposed above that matches the system, the processed data are shown in Supplemental Figure S6 (including the experimental process description).
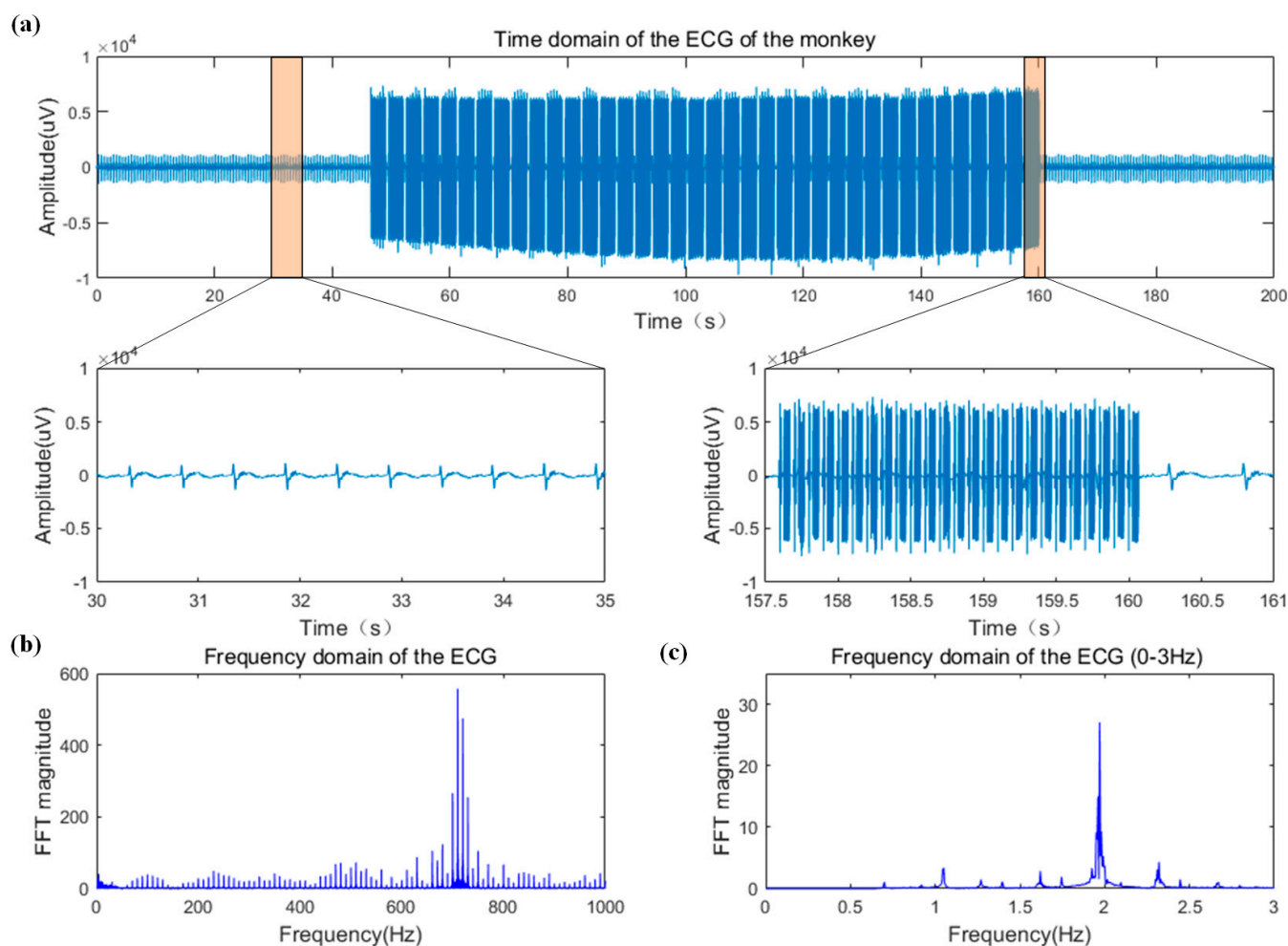
Figure 6. (**a**) ECG polluted by the gradient artifact in the time domain. The more specific signals in the orange boxes are shown below Figure 6a. (**b**) The signal is mixed with GA noise in the full band frequency domain. (**c**) ECG frequency domain of 0–3 Hz.

3.2.2. Comparison with TDT for Epilepsy Signal Acquisition in 7T MRI

To compare the effectiveness of the more recent test system in collecting EEG signals, we collected epileptic EEG signals from rats at 7T and made a magnetic-compatible synchronous acquisition interface to enable our device and commercial EEG device TDT System 3D to simultaneously collect signals for comparison. TDT is a commonly used magnetic compatible equipment, but its high price, large size, non-portability and unintegrated components limit its widespread use. In this experiment, the seizure signals of rats were synchronously collected by our device and TDT to verify the MRI compatibility of the device. The experimental surgical procedures are described in Supplemental Note S2. The acquisition process of the equipment is shown in Figure 7a. The rat was injected with penicillin, the acquisition box designed by us and the amplifier of TDT was placed in the 7T NMR chamber. In the chamber, epileptic EEG signals of the rat were collected through magnetically compatible ECOG electrodes, and the signals were simultaneously transmitted to our device and TDT amplifier through the synchronous interface outside the nuclear magnetic field. Signals from our equipment were received wirelessly, signals from the TDT amplifier were received wired and fMRI images were collected and drawn by the computer for the MRI equipment. Supplemental Figure S7 showed the comparison of normal EEG and epileptic EEG of rats under the non-NMR conditions compared with those signals from the TDT device. The experiments showed that our device and the TDT device could collect similar effective EEG signals at the same time.
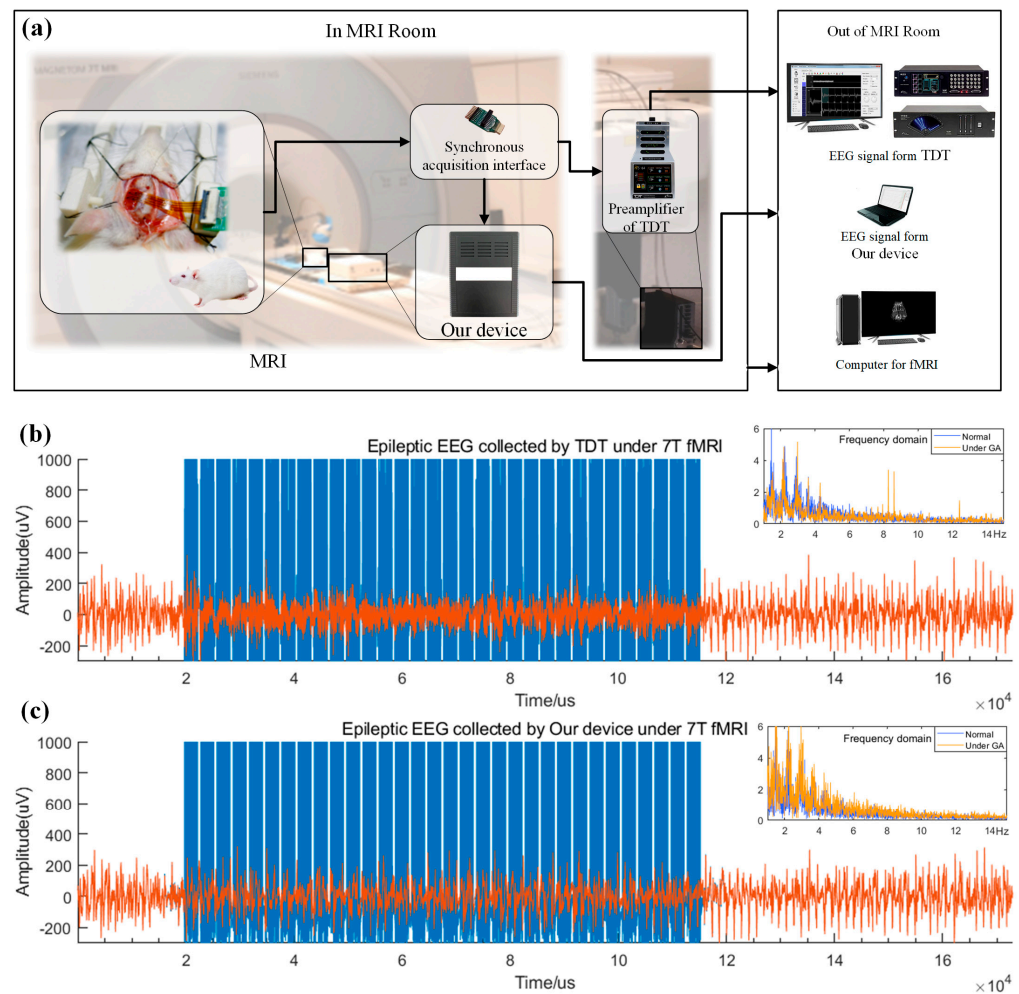
Figure 7. (**a**) TDT amplifier and our equipment simultaneously collect epileptic signals from rats under anesthesia to verify the consistency of signal collection under 7T fMRI. (**b**,**c**) The EPI scan sequence under 7T fMRI simultaneously collected by the TDT amplifier and our device. The blue signal is the original signal, and the red signal is the EEG signal of epileptic rats after removing the gradient artifact from the original data. The right sides of (**b**,**c**) are the frequency domain information obtained by the FFT transformation of the EEG. The yellow signal is the frequency domain information of the EEG in the original signal after the removal of the gradient artifacts, while the blue signal is the frequency domain information without the influence of the gradient artifacts.

Furthermore, under 7T fMRI, TDT and our equipment simultaneously collected induced epileptic signals from rats under anesthesia to verify the consistency of the signal collection, demonstrating the ability of EEG32 for synchronous MRI scanning, signal acquisition and the removal of MRI scanning artifacts. Figure 7b,c respectively show 32 slices under a volume of EPI scan sequence simultaneously collected by the commercial magnetic compatible device TDT amplifier and our designed device under the synchronous acquisition interface. The blue signal is the original signal collected by the device, and the red signal is the EEG signal of epileptic rats after removing the gradient artifact. The right sides of Figure 7b,c are the frequency domain information obtained by the FFT transformation of the EEG. The yellow signal is the frequency domain information of the EEG under the influence of gradient artifacts in the original EEG after the removal of gradient artifacts, while the blue signal is the frequency domain information without the influence of gradient artifacts. The RMSE is used to calculate the change in the signal distribution in the frequency domain under the influence of gradient artifacts to measure the effectiveness of the signal collected by the TDT and our device. The TDT device has 0.3708 RMSE, while

our device has 0.3354 RMSE. It can be proven that our device can collect EEG signals under 7T fMRI operation, and effective EEG signals can be obtained through LOGDAE designed by us. The lower MAE value indicates that the quality of the EEG signals collected by our device is better than that of commercial TDT devices under nuclear magnetic interference.

4. Conclusions

This article provides a 256-channel, portable, high-performance, low-input noise, 7T MRI-compatible acquisition system that is compatible with a variety of EP signals, including ECG, EMG, EEG and ECoG signals. With input noise below 1 μVrms and a dynamic range of ±225 mV, it ensures precise and powerful signal acquisition. Specially engineered shields for lead wires, equipment and PCBs enhance the safety and minimize the artifacts in the MRI environment. The system's streamlined design allows for acquisition and digitization within a 20 cm × 13 cm × 8 cm space, providing portability and the possibility of more applications. Through empirical testing, the system demonstrates proficiency in collecting various EP signals both within and beyond the MRI setting, effectively eliminating gradient artifacts. Equipped with data processing software and artifact removal algorithms, it delivers cleaner and more accurate results. The performance of acquisition equipment that can adapt to a variety of occasions, and the convenience and possibility it brings are worth further exploring. On the one hand, its adaptability enables a seamless transition between scenarios by swapping electrodes, promising convenience and versatility. In the realm of innovation, this system stands as a gateway to enhanced EP signal acquisition, offering a promising avenue for exploration and application.

Supplementary Materials: The following supporting information can be downloaded at https://www.mdpi.com/article/10.3390/electronics12173648/s1: Supplemental Note S1: Schematic diagram of the overall acquisition system composition; Supplemental Note S2: Experiment animals and surgery; Figure S1: MRI EPI scan sequence synchronization signal acquisition module; Figure S2: LOGDAE model and training and test results of LOGDAE; Figure S3: ECG recording with a sensor position corresponding to V4; Figure S4: Four-channel sEMG recording displayed on the computer user interface for surface EMG recordings; Figure S5: PEDOT:PSS electrode to record the sinusoidal signal generated by a physiological signal generator; Figure S6: Heart rate monitoring by the ECG in 7T MRI after removing the gradient artifacts by LOGDAE; Figure S7: The comparison of normal EEG and epileptic EEG of rats under the non-NMR conditions compared with those signals from the TDT device; Table S1: The performance parameters of our device are compared with commercial equipment; Table S2: Amplitude and frequency range of the electrophysiological signal.

Author Contributions: Conceptualization, J.P.; methodology, J.X.; data curation, F.Z.; writing—original draft preparation, J.P. and J.X.; writing—review and editing, F.Z.; investigation, L.Z.; project administration, S.Z. and S.D. and funding acquisition, G.P. All authors have read and agreed to the published version of the manuscript.

Data Availability Statement: The data presented in this study are available on request from the corresponding author. The data are not publicly available due to privacy.

Conflicts of Interest: The authors declare no conflict of interest.

References

1. Logothetis, N.K. What we can do and what we cannot do with fMRI. *Nature* **2012**, *453*, 869–878. [CrossRef] [PubMed]
2. Schulz, K.; Sydekum, E.; Krueppel, R.; Engelbrecht, C.J.; Schlegel, F.; Schroter, A.; Rudin, M.; Helmchen, F. Simultaneous BOLD fMRI and fiber-optic calcium recording in rat neocortex. *Nat. Methods* **2012**, *9*, 597–607. [CrossRef] [PubMed]
3. Kosten, L.; Emmi, S.A.; Missault, S.; Keliris, G.A. Combining magnetic resonance imaging with readout and/or pertur-bation of neural activity in animal models: Advantages and pitfalls. *Front. Neurosci.* **2022**, *16*, 938665. [CrossRef] [PubMed]

4.　Sclocco, R.; Garcia, R.G.; Kettner, N.W.; Isenburg, K.; Fisher, H.P.; Hubbard, C.S.; Ay, I.; Polimeni, J.R.; Goldstein, J.; Makris, N.; et al. The influence of respiration on brainstem and cardiovagal response to auricular vagus nerve stimulation: A multimodal ultrahigh-field (7T) fMRI study. *Brain Stimul.* **2019**, *12*, 911–921. [CrossRef]

5.　Ebrahimzadeh, E.; Shams, M.; Fayaz, F.; Rajabion, L.; Mirbagheri, M.; Nadjar Araabi, B.; Soltanian-Zadeh, H. Quantitative determination of concordance in localizing epileptic focus by component-based EEG-fMRI. *Comput. Methods Programs Biomed.* **2019**, *177*, 231–241. [CrossRef]

6.　Lioi, G.; Butet, S.; Fleury, M.; Bannier, E.; Lecuyer, A.; Bonan, I.; Barillot, C. A Multi-Target Motor Imagery Training Using Bimodal EEG-fMRI Neurofeedback: A Pilot Study in Chronic Stroke Patients. *Front. Hum. Neurosci.* **2020**, *14*, 37. [CrossRef]

7.　Cecchetti, G.; Agosta, F.; Canu, E.; Basaia, S.; Barbieri, A.; Cardamone, R.; Bernasconi, M.P.; Castelnovo, V.; Cividini, C.; Cursi, M.; et al. Cognitive, EEG, and MRI features of COVID-19 survivors: A 10-month study. *J. Neurol.* **2022**, *269*, 3400–3412. [CrossRef]

8.　Perlaki, G.; Orsi, G.; Schwarcz, A.; Bodi, P.; Plozer, E.; Biczo, K.; Aradi, M.; Doczi, T.; Komoly, S.; Hejjel, L.; et al. Pain-related autonomic response is modulated by the medial prefrontal cortex: An ECG-fMRI study in men. *J. Neurol. Sci.* **2015**, *349*, 202–208. [CrossRef]

9.　Schrooten, M.; Vandenberghe, R.; Peeters, R.; Dupont, P. Quantitative Analyses Help in Choosing Between Simultaneous vs. Separate EEG and fMRI. *Front. Neurosci.* **2019**, *12*, 11. [CrossRef]

10.　Angelone, L.M.; Vasios, C.E.; Wiggins, G.; Purdon, P.L.; Bonmassar, G. On the effect of resistive EEG electrodes and leads during 7 T MRI: Simulation and temperature measurement studies. *Magn. Reson. Imaging* **2006**, *24*, 801–812. [CrossRef]

11.　Jorge, J.; Grouiller, F.; Ipek, O.; Stoermer, R.; Michel, C.M.; Figueiredo, P.; van der Zwaag, W.; Gruetter, R. Simultaneous EEG-fMRI at ultra-high field: Artifact prevention and safety assessment. *Neuroimage* **2015**, *105*, 132–144. [CrossRef] [PubMed]

12.　Mullinger, K.J.; Castellone, P.; Bowtell, R. Best current practice for obtaining high quality EEG data during simultane-ous FMRI. *J. Vis. Exp.* **2013**, *1*, 50283.

13.　Angelone, L.M.; Potthast, A.; Segonne, F.; Iwaki, S.; Belliveau, J.W.; Bonmassar, G. Metallic electrodes and leads in sim-ultaneous EEG-MRI: Specific absorption rate (SAR) simulation studies. *Bioelectromagnetics* **2004**, *25*, 285–295. [CrossRef] [PubMed]

14.　Ritter, P.; Villringer, A. Simultaneous EEG-fMRI. *Neurosci. Biobehav. Rev.* **2006**, *30*, 823–838. [CrossRef]

15.　Huster, R.J.; Debener, S.; Eichele, T.; Herrmann, C.S. Methods for simultaneous EEG-fMRI: An introductory review. *J. Neurosci.* **2012**, *32*, 6053–6060. [CrossRef]

16.　Allen, P.J.; Josephs, O.; Turner, R. A method for removing imaging artifact from continuous EEG recorded during func-tional MRI. *Neuroimage* **2000**, *12*, 230–239. [CrossRef]

17.　Liu, Z.; de Zwart, J.A.; van Gelderen, P.; Kuo, L.W.; Duyn, J.H. Statistical feature extraction for artifact removal from concurrent fMRI-EEG recordings. *Neuroimage* **2012**, *59*, 2073–2087. [CrossRef]

18.　Xia, H.; Ruan, D.; Cohen, M.S. Removing ballistocardiogram (BCG) artifact from full-scalp EEG acquired inside the MR scanner with Orthogonal Matching Pursuit (OMP). *Front. Neurosci.* **2014**, *8*, 218. [CrossRef]

19.　Luo, Q.; Huang, X.; Glover, G.H. Ballistocardiogram artifact removal with a reference layer and standard EEG cap. *J. Neurosci. Methods* **2014**, *233*, 137–149. [CrossRef]

20.　Niazy, R.K.; Beckmann, C.F.; Iannetti, G.D.; Brady, J.M.; Smith, S.M. Removal of FMRI environment artifacts from EEG data using optimal basis sets. *Neuroimage* **2005**, *28*, 720–737. [CrossRef]

21.　Sing, S.P.; Mishr, S.; Gupt, S.; Padmanabha, P.; Ji, L.; Colin, T.K.A.; Tsai, Y.T.; Kejia, T.; Sankarapillai, P.; Mohan, A. Func-tional Mapping of the Brain for Brain–Computer Interfacing: A Review. *Electronics* **2023**, *12*, 604. [CrossRef]

22.　Amprimo, G.; Rechich, I.; Ferrari, C.; Olm, G. Measuring Brain Activation Patterns from Raw Single-Channel EEG during Exergaming: A Pilot Study. *Electronics* **2023**, *12*, 623. [CrossRef]

23.　Hwang, J.; Park, S.; Chi, J. Improving Multi-Class Motor Imagery EEG Classification Using Overlapping Sliding Window and Deep Learning Model. *Electronics* **2023**, *12*, 1186. [CrossRef]

24.　Kang, Q.; Li, F.; Gao, J. Exploring the Functional Brain Network of Deception in Source-Level EEG via Partial Mutual Infor-mation. *Electronics* **2023**, *12*, 1633. [CrossRef]

25.　Duffy, B.A.; Toga, A.W.; Kim, H. Gradient Artifact Correction for Simultaneous EEG-fMRI using Denoising Auto-encoders. *IEEE Int. Symp. Biomed. Imaging* **2020**, *1*, 1408–1411.

26.　Folgado, D.; Barandas, M.; Antunes, M.; Nunes, M.L.; Liu, H.; Hartmann, Y.; Schultz, T.; Gamboa, H. Tssearch: Time series subsequence search library. *SoftwareX* **2022**, *18*, 101049. [CrossRef]

27.　Rodrigues, J.; Liu, H.; Folgado, D.; Belo, D.; Schultz, T.; Gamboa, H. Feature-Based Information Retrieval of Multimodal Biosignals with a Self-Similarity Matrix: Focus on Automatic Segmentation. *Biosensors* **2022**, *12*, 1182. [CrossRef]

28.　Correa, A.G.; Laciar, E.; Patiño, H.D.; Valentinuzzi, M.E. Artifact removal from EEG signals using adaptive filters in cascade. *J. Phys. Conf. Series* **2007**, *1*, 90. [CrossRef]

29.　Grouiller, F.; Vercueil, L.; Krainik, A.; Segebarth, C.; Kahane, P.; David, O. A comparative study of different artefact re-moval algorithms for EEG signals acquired during functional MRI. *Neuroimage* **2007**, *38*, 124–137. [CrossRef]

30.　Schlag, M.G.; Hopf, R.; Redl, H. Serial recording of sensory, corticomotor, and brainstem-derived motor evoked poten-tials in the rat. *Somatosens. Mot. Res.* **2001**, *18*, 106–116.

31. Yizhar, O.; Fenno, L.E.; Davidson, T.J.; Mogri, M.; Deisseroth, K. Optogenetics in neural systems. *Neuron* **2011**, *71*, 9–34. [CrossRef] [PubMed]

32. Zhang, F.; Zhang, L.; Xia, J.; Zhao, W.; Dong, S.; Ye, Z.; Pan, G.; Luo, J.; Zhang, S. Multimodal Electrocorticogram Active Electrode Array Based on Zinc Oxide-Thin Film Transistors. *Adv. Sci.* **2023**, *10*, e2204467. [CrossRef] [PubMed]